INSTITUTE OF PHYSICS PUBLISHING JOURNAL OF OPTICS A: PURE AND APPLIED OPTICS

J. Opt. A: Pure Appl. Opt. **4** (2002) S304–S310 PII: S1464-4258(02)37569-X

Signal processing and testing of displacement metrology gauges with picometre-scale cyclic nonlinearity

Peter G Halverson and Robert E Spero

Jet Propulsion Laboratory, California Institute of Technology, Pasadena, CA 91109, USA

E-mail: Peter.Halverson@jpl.nasa.gov

Received 27 May 2002
Published 4 November 2002
Online at stacks.iop.org/JOptA/4/S304

Abstract

The Space Interferometry Mission (see http://sim.jpl.nasa.gov) requires displacement metrology gauges with linearity ∼10 pm rms over a distance of several metres. Displacement measuring interferometers are under development to meet these requirements, while also meeting thermal stability, robustness, size and geometry requirements. A persistent difficulty in attaining picometre-class performance with laser interferometric metrology gauges is the problem of 'cyclic error' which may be caused by small amounts of mixing of the interferometer measurement and reference signals. The mixing is caused by crosstalk, both optical and electronic. Other causes of cyclic error have been also found and will be discussed.

This paper describes our approach to minimizing the cyclic error with emphasis on signal processing issues and the concurrent development of techniques to detect the error as it is gradually reduced to zero.

Keywords: Displacement metrology, metrology gauges, interferometry, astrometry, cyclic error, cyclic nonlinearity

1. Introduction

Ultra-precise relative distance measurements are needed to monitor (and possibly control) the geometry of the telescope array and starlight transfer optics of the Space Interferometry Mission (SIM) [1, 2] scheduled for launch in 2009. SIM will repeatedly measure the relative angular positions of ∼2000 stars to 5 prad accuracy over five years. These data will allow the detection and characterization of planets orbiting the stars, will provide accurate stellar distance and velocity determinations and provide new insights into the character and distribution of the invisible 'dark matter' thought to permeate the universe.

SIM's angular precision, $\delta\theta$, will be limited by the uncertainty, δL, in knowledge of the optics' geometry relative to $D = 10$ m, the optical baseline. For 5 prad accuracy, $\delta L = D\delta\theta = (10\text{ m})(5 \times 10^{-12}) = 50$ pm. To accommodate other sources of uncertainty, the error budgeted to the monitoring of optical displacement is only 10 pm. Meeting this goal has proven to be a challenge.

The 15 distance measurements used in SIM will define only the *angular* geometry of SIM, relaxing the absolute stability requirement on our distance standard: the $\lambda = 1319$ nm wavelength of a YAG laser source. This is because a change in laser wavelength will appear to the system as a change in scale, not a change in the angles between optics.

2. The metrology gauge

The laser heterodyne interferometer [3, 4] in figure 1 is a metrology gauge that measures L, the distance between two hollow corner cube retro-reflectors. A Michelson interferometer, it is similar to commercial gauges [5, 6], to those used in calibrating physical standards [7] and in dilatometry [8].

Changes in the relative phase Φ cycles of the heterodyne signals from the reference (R) and measurement (M) photodiodes inform us of changes in the optical path difference (OPD) between the reference and measurement beams. From this we obtain $\Delta L = \lambda\Delta\Phi/2$, the change in distance between the two corner cube fiducials.

The R and M signals are caused by the reference and measurement beams having optical frequencies that differ by

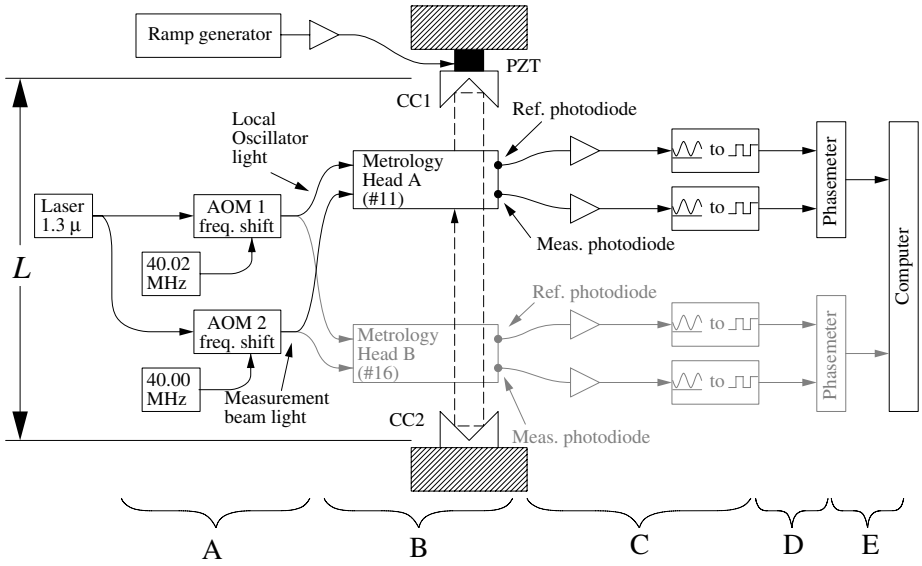

Figure 1. Block diagram of laser heterodyne interferometer which measures changes in L, the distance between retro-reflectors CC1 and CC2. An optional second gauge (shown in grey) can measure the same distance, allowing useful gauge comparisons. The letters A–E indicate regions where cyclic error originates and are discussed in the text. For cyclic error detection, the PZT actuator moves CC1 with a voltage ramp that has been precompensated for piezo hysteresis, to achieve near-constant velocity.

20 kHz, and interfere at the photodiodes. The frequency difference is imparted by acousto-optic modulators (AOMs) driven by RF signals at 40 and 40.02 MHz. The laser, AOMs and metrology heads are all interconnected by polarization maintaining fibre.

The photodiodes and preamps are of a commercial design [9], modified for use in vacuum. The transimpedance gain for these experiments was 15 kΩ, and the peak-to-peak amplitude of the heterodyne sinusoid at the preamp outputs varied between channels from 1 to 4 V. The channel-to-channel variation in signal strengths was due to details of the optics internal to the metrology heads.

The measurement of Φ is carried out by converting the R and M signals from sinusoid to square wave (TTL logic levels) using zero-crossing detectors preceded by bandpass filters. Φ is calculated by a custom phasemeter [10] as the time delay between the R and M transition, which is later divided (using software) by the heterodyne period to convert to cycles. The phasemeter's digitization resolution is 7.8 ns, giving a single measurement gauge resolution of 102 pm. However, the phasemeter measures the phase of every zero crossing (20 000 per second) and performs on-board averaging. For these experiments, the phasemeter was read out at 25 Hz, hence each datum is the average of 800 phase measurements, which greatly reduces the effects of photodiode and electronic noise, and enhances the resolution of the phase determination.

The gauges are designed for use in vacuum and were tested in a vacuum chamber (operated at 1 atm), hence the optical fibres and signal cables pass through vacuum feedthroughs, which complicates the task of minimizing crosstalk. Further details regarding the apparatus can be found in [11].

3. Types of error

Interferometric displacement gauges are susceptible to various errors. Briefly, these are as follows.

(1) Cyclic error: this is discussed in the next section.
(2) Diffraction error: the gauges under consideration here are intended for small dynamic range. L will change by $\Delta L < 10\ \mu$m, out of $L \sim 10$ m. The resulting change has been calculated to give <1 pm of error, linear in ΔL.
(3) Mispointing: L will have an error $e = L\theta^2$ if θ, the mispointing angle between the measurement beam and the optical axis between retro-reflectors, is non-zero. It is possible to minimize this error by the use of an automatic pointing system [12].
(4) Thermal drift: temperature changes (a) in the metrology head can affect the optics and (b) in the preamps and filters can change signal phase delays.
(5) Laser drift: changes in λ appear to the system as distance changes.
(6) Various noise sources: vibrations, photodiode shot noise, amplifier noise and phasemeter digitization.

Our current emphasis is on estimating error source (1), the cyclic nonlinearity. By operating the interferometer in a nominally static configuration, the measurement error from sources (3)–(6) was determined to be less than 10 pm total (table 1). We now consider error source (1), the cyclic nonlinearity.

4. Cyclic error

When the distance measured is varied, interferometric displacement gauges exhibit a nonlinearity, illustrated in figure 2, that is periodic in $\lambda/2$. This effect has been studied in depth [13–17] and progress made, resulting in errors of less than 10 pm rms [18]. However, these gauges do not satisfy the SIM requirement of measuring the separation between fiducials mechanically distinct from the metrology head.

Briefly, cyclic error is caused by mixing of the reference and measurement signals (see figure 1). If a portion,

Table 1. Summary of results derived from data of figure 9. Units are picometres rms of cyclic error. Data for the higher harmonics are not shown, but are discussed in the text.

Head number	Calibration amplitude	A = with-motion amplitude	B = no-motion amplitude	Difference C = A − B	Difference C rescaled
		First harmonic, 2.07–2.10 Hz			
#11	956	16	10	13	13
#16	965	19	10	17	17
Difference	1753	12	5	12	7
		Second harmonic, 4.17–4.20 Hz			
#11	867	17	8	15	17
#16	866	13	8	11	13
Difference	1270	15	3	14	11
		Third harmonic, 6.23–6.27 Hz			
#11	818	10	7	8	10
#16	818	10	6	8	10
Difference	534	3	3	∼0	∼0

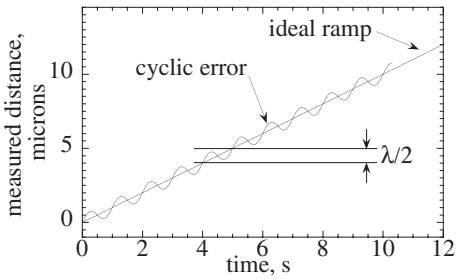

Figure 2. Cyclic error appears as a sinusoidal deviation from expected measurement, periodic in $\lambda/2$, $\lambda/4 \ldots \lambda/2n$, when the distance between fiducials is increased linearly. Near-linear motion is introduced using the ramp generator and PZT in figure 1.

of amplitude a_R, of the reference signal contaminates the measurement signal of amplitude A_M, the resulting error will be (see [16], equation (1))

$$\varepsilon_1 \approx \frac{1}{\sqrt{2}} \frac{\lambda}{2} \frac{1}{2\pi} \frac{a_R}{A_M} \approx \frac{\lambda}{18} \frac{a_R}{A_M} \tag{1}$$

where the constants account for conversion to rms, the measurement beam's double-pass through L, and the peak phase shift the signal of amplitude a_R can impart to the sinusoidal signal of amplitude A_M. In addition to this, there will usually be mixing in the other direction, resulting in an error

$$\varepsilon_2 \approx \frac{\lambda}{18} \frac{a_M}{A_R}. \tag{2}$$

It is difficult to determine the relative phase between ε_1 and ε_2, so we can set only an upper limit on the combined effect. For SIM, where $\varepsilon < 10$ pm and $\lambda = 1.3$ μm, we must have the mixing $a/A < 10^{-4}$, i.e. the signals must be isolated to better than 80 dB. Because mixing occurs through multiple mechanisms, we try to limit the leakage from any single source to < -90 dB.

We now consider sources of cyclic error in the JPL system by regions A, B, C, ... as indicated in figure 1.

4.1. Frequency shifters, RF leakage

The gauge's laser light is split into two paths and frequency shifted to create two optical frequencies separated by F_{het}, the system heterodyne frequency (=20 kHz, see figure 1). The frequency shifters are fibre-coupled AOMs that have peak efficiency at 40 MHz. Thus the RF for the first, 'local oscillator' path, is 40.02 MHz, while for the second, 'measurement' path it is 40.00 MHz. Mixing of the RF signals causes cyclic error with a magnitude as predicted by equation (1).

110 dB isolation was achieved using separate (but synchronized) signal generators and RF amplifiers. A noticeable improvement occurred when the coaxial cables connecting the RF amplifiers to the AOMs were upgraded from RG-58 to heavily shielded RG-142 and when the AOMs were isolated from the aluminium breadboard. This may be due to the elimination of a ground loop where the first RF cable's shield acted as a return path for the second RF source's signal, and vice versa.

4.2. Metrology head, optical mixing

In the interferometer metrology head [19, 20] the measurement beam travels the distance between the corner cube fiducials and is mixed with the local oscillator beam at the measurement photodiode, which produces a heterodyne beat signal. A separate portion of the measurement beam goes directly to the reference photodiode where it mixes with the local oscillator, producing a reference signal against which the measurement signal is compared. Any leakage of beams into unintended paths (e.g. a local oscillator travelling to the fiducials) will cause cyclic error with amplitude

$$\varepsilon \approx \frac{\lambda}{18} \frac{a}{A} = \frac{\lambda}{18} \left(\frac{p}{P} \right)^{1/2}, \tag{3}$$

where p/P is the ratio of leakage power to 'good' beam power.

In typical polarizing metrology systems the isolation between beams is only ∼30 dB, resulting in ∼2 nm cyclic errors. The present metrology head maintains a physical separation of the beams, achieving >70 dB isolation. The exact performance of these optics is unknown, and its characterization is the final product of our test facility.

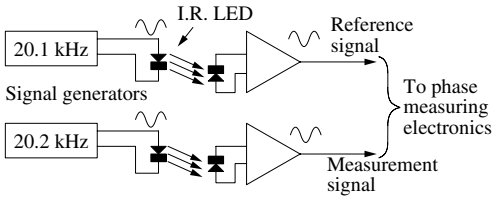

Figure 3. Signal generators driving infrared LEDs produce simulated interference light to test the metrology photodiodes and associated electronics. A spectrum analyser (HP 89410A) connected to the reference output will observe the expected 20.1 kHz from the first signal generator and a small amount of 20.2 kHz leakage from the second. (Care must be taken to isolate the signal generators from the rest of the electronics.) Such explorations also find other sources of contamination such as noise from nearby computers, clock signals etc.

4.3. Photodiode signal mixing

Electrical isolation was achieved by operating the photodiode preamps, filter and sine-to-square wave converters on independent power supplies, and by preventing ground loops. The reference and measurement channels have shields and grounds which connect only at the phasemeter inputs.

Improvement was also obtained by reducing the heterodyne frequency to the present 20 kHz, instead of 100 kHz. This is probably due to a reduction in capacitive coupling effects which grow linearly with frequency. Further improvement was made by eliminating termination resistors at the filter inputs which minimized the current flowing out of the preamps. A final improvement (not yet implemented) would be replacement of the single-ended filter inputs with differential inputs.

The combined effect of these steps was to bring the signal leakage down to -90 dB (from -70 dB). The cyclic error measured with the simulated signals, using the analysis methods described below, was 1 pm.

Identifying signal mixing at these low levels and verifying >90 dB isolation required the creation of well separated, heterodyne signals with unique frequencies as shown in figure 3. Crosstalk between signal paths was monitored using a HP 89410A spectrum analyser.

4.4. Timing signal mixing

The outputs of the sine-to-square-wave converters are 5 V TTL logic signals. While these are inherently immune to crosstalk effects, it was found that the 50 Ω termination at the phasemeter inputs caused large current flows that appeared as contamination in the photodiode preamp outputs, resulting in cyclic error at twice the usual frequency. This problem was also seen with other logic signals, such a 20 kHz reference clock. Eliminating the 50 Ω terminations (and substituting 50 Ω series resistances at the outputs to prevent second reflections), brought the contamination from this source down to -125 dB.

4.5. Phasemeter time-of-measurement error

The gauge's phasemeter measures the relative time ΔT of logic transitions signalling the zero-crossings of the photodiode signals (after removal of DC offsets). This approach creates an ambiguity as to when the phase measurement

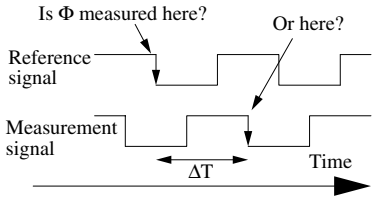

Figure 4. Heterodyne signals, converted to square waves, have their relative phases measured by comparing times of falling edges. The *time* at which the phase is determined has an ambiguity ΔT which causes a significant cyclic error if Φ is changing rapidly.

are made, as illustrated in figure 4. The time of phase measurement is important when the phase is changing—as in these experiments, where the phase is changing linearly at a rate ν cycles per second. The reference phase changes slowly, so the effect is in the phase of the measurement signal. The error is

$$\frac{\lambda}{2}\Delta\Phi = \frac{\lambda}{2}\nu\Delta T = \frac{\lambda}{2}\frac{\nu}{F_{\text{het}}}\text{fract}(\Phi), \tag{4}$$

where Fract(Φ) is the fractional part of the phase difference, ranging from 0 to 1 cycle. This error is cyclic, since Fract(Φ) is periodic in Φ, and is observed as a deviation from the ideal measurements, similar to figure 2, but with a sawtooth error signal. The peak-to-peak amplitude is 66 pm, for the $\nu = 2$ cycles per second actuation velocity used in these experiments.

This error is easily removed by subtraction:

$$\Phi_{\text{corrected}} = \Phi - \frac{\nu}{F_{\text{het}}}\text{Fract}(\Phi), \tag{5}$$

a procedure implemented with software. The effectiveness of this correction was verified with test signals, and the residual error is <1 pm.

5. Detecting cyclic error

Cyclic nonlinearity is manifested as a periodic deviation from the linear ramp expected when constant velocity motion is applied to one of the endpoint fiducials. This underlies the method used for detecting and measuring the cyclic nonlinearity. The JPL test facility includes a piezoelectric (PZT) actuator to move one of the fiducials.

The system in figure 1 can test two metrology gauges simultaneously. This is possible because the measurement beams travel in a 'racetrack' path: the upward path is offset 2 cm from the downward path, allowing the propagation of beams from two gauges without interference. Simultaneous measurements allows subtraction of common-mode noise (laser drift, optical table vibrations).

Figure 5 shows typical data from this system (using only one gauge). The ramp linearly decreases the distance between fiducials. To find the cyclic error we begin by subtracting a linear fit to the distance data:

$$L_{\text{D}}(t) = L(t) - (mt + b). \tag{6}$$

The residuals in L_{D} are dominated by a slow $\sim$1% deviation from linearity in the piezo ramp. The cyclic error is the $\sim$2 Hz sinusoid, just visible above the noise from air fluctuations and mechanical vibrations.

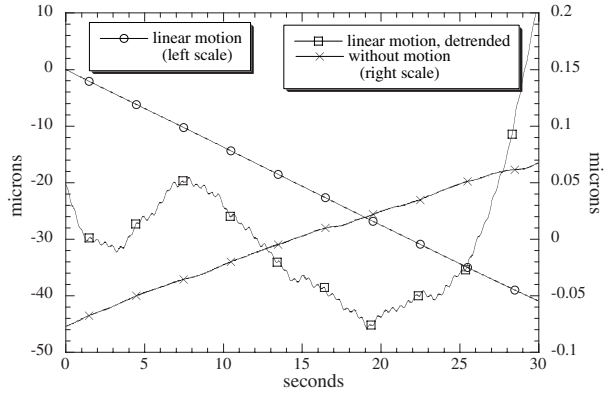

Figure 5. Typical nonlinearity test data showing the ∼40 μm near-linear motion of the retro-reflector and the same data, detrended and magnified by 100, revealing deviations from linear motion caused by piezo non-linearity (parabola-like effect) and gauge cyclic nonlinearity (small 2 Hz sinusoid). The corner cube position was not actuated in the 'without motion' curve, to reveal noise sources unassociated with the actuation. The small, ∼0.15 μm, linear trend is caused by PZT creep.

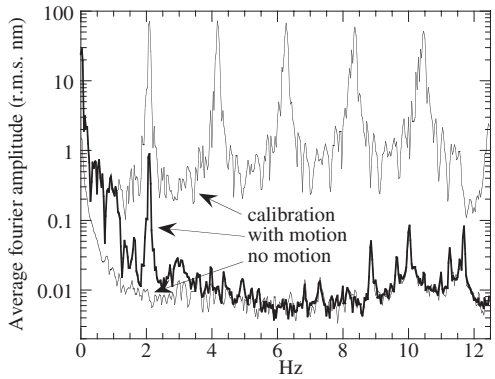

Figure 6. rms averages of the amplitudes of 100 Fourier transforms. Middle, bold, trace: average magnitude of Fourier transforms of detrended with-motion data similar to figure 5. Note that around the frequency $2\nu/\lambda = 2.2$ Hz a ∼1 nm cyclic nonlinearity 'peak' is evident. Bottom trace: data with no linear motion. Top trace: detrended, with-motion data, same as middle trace, but with calibration peaks added by software (see text).

6. Measuring the cyclic error amplitude

The prominent peak in figure 6, middle trace, is at a frequency equal to the rate of fringe passage in the metrology head, 2.2 Hz: the peak is due to cyclic error and not to spurious effects such as mechanical vibrations. The rms sum of the amplitude bins under the peak yields the amplitude of the cyclic error: $\varepsilon = 1.2$ nm rms.

The with-motion data in figure 6 exhibit a higher noise level, at all frequencies, than the no-motion data. This is due to imperfect PZT ramp electronics (DAC noise leaking past 1 Hz low-pass filters) and excitation of resonances at the sweep start. This excess noise will ultimately limit the cyclic error detection threshold of the system.

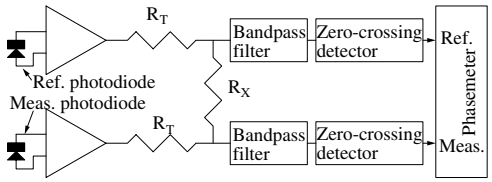

Figure 7. Setup to introduce a known amount of crosstalk for exercising the cyclic error measurement technique. Resistance $R_X (= 10\ \mathrm{k}\Omega)$ causes the reference and measurement signals to mix. Termination resistances R_T are 50 Ω.

6.1. Insertion of test cyclic error

The cyclic error in figures 5 and 6 had been deliberately worsened by adding resistance R_X between termination resistors R_T, creating a path for crosstalk between the Reference and Measurement signals in figure 7.

The rms cyclic error added by this resistance can be predicted:

$$\varepsilon = \frac{1}{\sqrt{2}}(\Delta\phi_R + \Delta\phi_M)\frac{(\lambda/2)}{2\pi} \tag{7}$$

where $\Delta\phi_R$ and $\Delta\phi_M$ are shifts in phase of the zero-crossing (we only use the rising part of the sinusoid). These will be

$$\Delta\varphi_R = \frac{R_T}{R_X}\frac{A_M}{A_R} \qquad \text{and} \qquad \Delta\varphi_M = \frac{R_T}{R_X}\frac{A_R}{A_M}, \tag{8}$$

where $A_R (= 4.3$ V) and $A_M (= 1.0$ V) are the peak-to-peak signal amplitudes out of the reference and measurement preamps, respectively. Finally, we have

$$\varepsilon = \frac{\lambda}{4\pi\sqrt{2}}\frac{R_T}{R_X}\left(\frac{A_R^2 + A_M^2}{A_R A_M}\right) = 1.7\ \text{nm}. \tag{9}$$

6.2. Calibration

A calibration signal is added by software to Φ, the phase data (in cycles) from the experiment:

$$\Phi' = \Phi + \frac{\sqrt{2}\varepsilon_{cal}}{\lambda/2}\sum_{n=1,\ldots,5}\sin(2n\pi\,\mathrm{fract}(\Phi)). \tag{10}$$

The effect of this added signal is shown in the top trace of figure 6, with $\varepsilon_{cal} = 100$ nm. The peaks indicate where errors periodic in Φ are expected for $n = 1 \ldots 5$. The calibration signal created by equation (10) has the same frequency distribution as the 'real' cyclic error, because they both have constant phase relative to Φ. Consequently, any spread in the 'real' peaks or drift in the peaks' frequency due to PZT hysteresis is also observed in the calibration peaks, guiding the analysis.

The search for peaks at high n is motivated by the observation that cyclic error sometimes manifests higher 'harmonics'. An effect at $n = 2$ is usually due to simultaneous leakage of local oscillator (figure 1) light into measurement light and vice versa. (It is also created by crosstalk between reference and measurement signal *after* conversion to square waves.) Leakage that makes n trips around the 'racetrack' appears as cyclic error at the nth peak. The current metrology

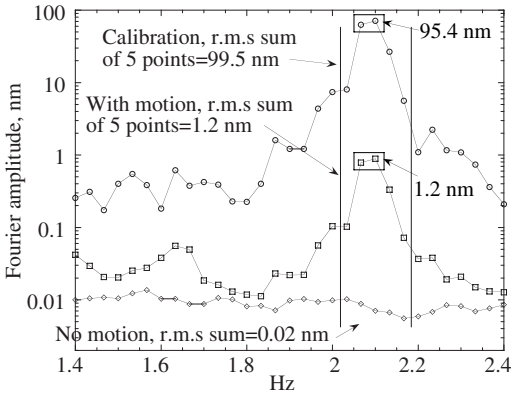

Figure 8. Same data as in figure 6, with expanded frequency scale. Note the agreement between calibration and 'real' cyclic error frequency distributions.

head design does not allow multiple round trips of any beams, hence $n > 2$ cyclic errors of optical origin are not expected.

Comparison of the 'real' $n = 1$ peak (due to R_X) with the first calibration peak in figure 6 reveals that the calibration peak is a good predictor of the frequency distribution of the cyclic error, as seen in figure 8.

Computation of the cyclic error may be accomplished in two ways. The first is the calculation of the rms sum under the peak: e.g. including just the five points between the bars in figure 8. This yields 99.5 nm for the 100 nm software-generated calibration. Computing the equivalent sum for the 'real' peak gives 1.2 nm, a measure of the cyclic error for the gauge. For better accuracy, we can subtract (in quadrature) the rms sum for the no-motion data, 0.2 nm, again giving 1.2 nm. (For measurements with smaller cyclic errors, subtracting the no-motion data will have a significant effect.)

A second method to compute the cyclic error, less affected by the broad-band noise introduced by the linear ramp, is to compute

$$\varepsilon = (A^2_{\text{cyclic}} - A^2_{\text{no motion}})^{1/2} \frac{\varepsilon_{\text{cal}}}{A_{\text{cal}}}, \qquad (11)$$

where ε_{cal} is the calibration cyclic amplitude, A_{cal} is the peak calibration amplitude point (or pair of points), A_{cyclic} is the same frequency 'real data' amplitude and $A_{\text{no motion}}$ is the corresponding 'no-motion' background amplitude. For the test data above, this gives $\varepsilon = (1.2^2 - 0.01^2)^{1/2}(100/95.4) = 1.2$ nm. This method will be applied to the following results.

7. Results

Six metrology heads fabricated by our industry partner, Lockheed–Martin, were tested and data for two typical units are presented here. Figure 9 shows data for the two units, that were acquired simultaneously, which will allow later removal of common-mode disturbances.

Each panel in figure 9 shows the rms average of Fourier amplitudes of data processed according to equation (6). The middle, bold traces have the 1.5 μm s^{-1} linear ramp which reveals cyclic error. The top traces are the same, but with the calibration cyclic error added. The bottom traces show data without the linear ramp, revealing the noise floor of the system,

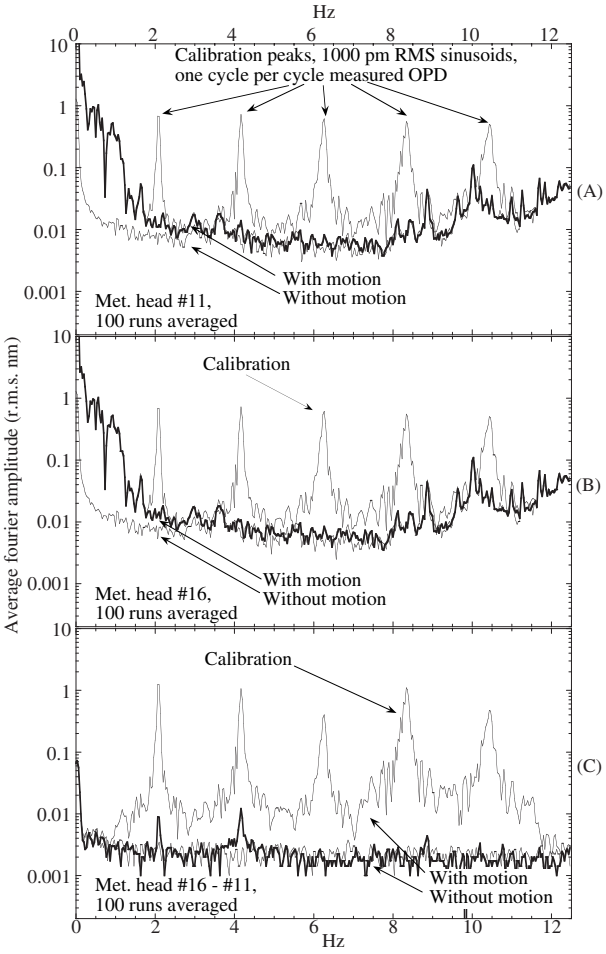

Figure 9. rms average of 100 amplitude spectra for gauges with metrology heads #11 (A) and #16 (B). Plot (C) is an average of amplitude spectra of the difference in simultaneous readings between the two gauges. For each plot, the bold trace shows detrended ~1.5 μm s^{-1} linear ramp data, the top trace shows the same data with 1 nm calibration 'cyclic error' added and the bottom trace shows no-motion background data.

including peaks from external sources of vibration (e.g. air handlers, pumps).

In table 1, the frequencies of the two highest amplitude points of each calibration peak were selected (as in figure 8) and are shown. The average amplitudes of all traces at the same frequencies are also shown. The last two columns show the cyclic error obtained by applying equation (11) to the results.

The last column of table 1 gives the cyclic error for each harmonic separately. Combining the first and second harmonics in quadrature yields a total rms cyclic error of 22 for metrology head number 11 and 21 pm for head number 16. These are upper limits to the error because some of the amplitude excess is caused by the overall increase in noise when the linear ramp is active. Since this noise is mechanical it is common to both gauges and is mostly eliminated in the difference of gauges, see figure 9(C).

In the difference of two gauges data, the combined first and second harmonics' cyclic error is 13 pm, and is the rms sum of the two gauges' error, which would be consistent with each gauge having 10 pm error. Unfortunately, we cannot determine with confidence how that error is allocated between

Table 2. Summary of cyclic error results. See text for discussion of assumptions involved in reaching 10 pm mean error conclusion.

Cyclic error upper limit:	$<$ 22 pm rms for each gauge
Mean cyclic error:	10 pm rms. One gauge may be higher, the other lower.

the two gauges, but the data support the claim that 22 pm and 21 pm errors are indeed upper limits.

For the third, fourth and fifth harmonics, the individual gauge results are dominated by the noise introduced by the ramp. For these frequencies the difference of gauges data is consistent with zero cyclic error. Since for this metrology head design we know of no mechanisms by which $n > 2$ cyclic error harmonics can be generated, we are confident that the errors are limited to the first two harmonics. These conclusions are summarized in table 2.

Analysis of the difference of gauges data must take the relative phases of the cyclic errors into account. It is entirely possible for the cyclic errors to disappear if the errors in the two gauges are of equal magnitude and phase. Fortunately, the two metrology heads have slightly different thickness optics so their signals are $\Delta\Phi = 133°$ apart, hence the cyclic errors will be magnified by $2\sin(n\Delta\Phi/2) = 1.83$ for $n = 1$, 1.47 for $n = 2$, 0.647 for $n = 3$, etc, resulting in the varied calibration peak amplitudes of figure 9(C). The validity of the claim of 10 pm mean error for two gauges depends on the 'real' cyclic error having the same underlying causes for each gauge, so that the phase of the cyclic error relative to the signal phase is the same for both gauges.

8. Conclusions

Implementation of displacement metrology gauges based on heterodyne interferometers, with linearity better than 100 pm, places stringent requirements both on the optics of the metrology heads, and on the supporting electronics and phase measuring apparatus. We have identified and corrected sources of cyclic nonlinearity in both domains resulting in a two order-of-magnitude improvement over commercial metrology gauges. The 10 pm rms linearity goal of the SIM appears to be within reach.

Acknowledgments

This research was carried out at the Jet Propulsion Laboratory, California Institute of Technology, under a contract with the National Aeronautics and Space Administration.

The authors wish to thank Raymond Savedra, John Shaw, Lawrence S Azevedo and Rosemary Diaz for their valuable technical support and Daniel MacDonald and Stuart Shaklan for their analysis and advice.

References

[1] SIM, Taking the Measure of the Universe *JPL publication* 400-811 3/99 (Available online at http://sim.jpl.nasa.gov/library/book.html)

[2] Unwin S and Shao M 2000 *Proc. SPIE (Munich, Germany)* vol 4006 p 754

[3] Zhao F *et al* 2001 Development of sub-nanometer racetrack laser metrology for external triangulation measurement for the space interferometry mission *Proc. ASPE 2001 Annual Meeting* (Arlington, VA: American Society for Precision Engineering) pp 349–52

[4] Gürsel Y 1993 Laser metrology gauges for OSI *Proc. SPIE Conf. on Spaceborne Interferometry (Orlando, FL)* ed Reasonberg *Proc. SPIE* **1947** 188–97

[5] ZMI 2000 *Displacement Measuring Interferometer Systems* (Middle Field, CT: Zygo Corp.) www.zygo.com

[6] HP 10716A *High-Resolution Interferometer*, Agilent Technologies, www.tm.agilent.com

[7] Gonda S *et al* 1999 Real-time, interferometrically measuring atomic force microscope for direct calibration of standards *Rev. Sci. Instrum.* **70** 3362–8

[8] Okaji M, Yamada N, Nara K and Kato H 1995 Laser interferometric dilatometer at low temperatures: application to fused silica SRM 739 *Cryogenics* **35** 887–91

[9] PDA400, Thorlabs, Inc., www.thorlabs.com

[10] Halverson P G, Johnson D R, Kuhnert A, Shaklan S B and Spero R 1999 A multichannel averaging phasemeter for picometer precision laser metrology *Proc. Conf. on Optical Engineering for Sensing and Nanotechnology (ICOSN '99, Yokohama, Japan) Proc. SPIE* **3740** 646–9

[11] Halverson P G, Azevedo L S, Diaz R T and Spero R E 2001 Characterization of picometer repeatability displacement metrology gauges *Proc. ODIMAP III, 3rd Topical Meeting on Optoelectronic Distance Measurement and Applications (Pavia, Italy)* pp 63–8

[12] Logan J E, Halverson P G, Regehr M W and Spero R E 2002 Automatic alignment of a displacement-measuring heterodyne interferometer *Appl. Opt.* **41** 4314–7

[13] Bobroff N 1987 Residual errors in laser interferometry from air turbulence and nonlinearity *Appl. Opt.* **26** 2676–82

[14] Augustyn W and Davis P 1990 An analysis of polarization mixing errors in distance measuring interferometers *J. Vac. Sci. Technol.* B **8** 2032–6

[15] Hou W and Wilkening G 1992 Investigation and compensation of the nonlinearity of heterodyne interferometers *Precision Eng.* **14** 91–8

[16] Wu C M and Su C S 1996 Nonlinearity in measurements of length by optical interferometry *Meas. Sci. Technol.* **7** 62–8

[17] Wu C M and Deslattes R D 1998 Analytical modeling of the periodic nonlinearity in heterodyne interferometry *Appl. Opt.* **37** 6696–700

[18] Lawall J and Kessler E 2000 Michelson interferometry with 10 pm accuracy *Rev. Sci. Instrum.* **71** 2669–76

[19] Zhao F *et al* 2001 Development of sub-nanometer racetrack laser metrology for external triangulation measurement for the Space Interferometry Mission *Proc. ASPE 2001 Annual Meeting* (Arlington, VA: American Society for Precision Engineering) pp 349–52

[20] Zhao F, Diaz R T, Halverson P G, Kuan G M and Shaklan S 2001 *Proc. ODIMAP III, 3rd Topical Meeting on Optoelectronic Distance Measurement and Applications (Pavia, Italy)* pp 39–44